Bubble Point Pressures of Binary Methanol/Water Mixtures in Fine-Mesh Screens

Jason Hartwig
Propellants and Propulsion Branch, NASA Glenn Research Center, Cleveland, OH 44135

J. Adin Mann
Emeritus Professor of Chemical Engineering, Case Western Reserve University, Cleveland, OH 44106

DOI 10.1002/aic.14293
Published online December 19, 2013 in Wiley Online Library (wileyonlinelibrary.com)

Binary methanol/water mixture bubble point tests involving three samples of fine-mesh, stainless steel screens as porous liquid acquisition devices are presented in this article. Contact angles are measured as a function of methanol mass fraction using the Sessile Drop technique. Pretest predictions are based on a Langmuir isotherm fit. Predictions and data match for methanol mole fractions greater than 50% when pore diameters are based on pure liquid tests. For all three screens, bubble point is shown to be a maximum at a methanol mole fraction of 50%. Model and data are in disagreement for mole fractions less than 50%, which is attributed to variations between surface and bulk fluid properties. A critical Zisman surface tension value of 23.2 mN/m is estimated, below which contact angles can be assumed to be zero. Solid/vapor and solid/liquid interfacial tensions are also estimated using the equation of state analysis from Neumann and Good. Published 2013 American Institute of Chemical Engineers *AIChE J*, 60: 730–739, 2014
Keywords: aqueous solutions, porous media, thermodynamics/classical, interfacial processes, multiphase flow

Introduction and Purpose

The purpose of this article is to present experimental results for the binary mixture bubble point tests conducted at the Cedar Creek Road Cryogenic Complex Cell 7 (CCL-7) at the NASA Glenn Research Center (GRC). As part of NASA GRC's ongoing liquid acquisition device (LAD) technology development program for cryogenic propulsion systems operating in low-gravity environments, three fine-mesh 304 stainless steel (304SS) screen channel LAD samples (325 × 2300, 450 × 2750, and 510 × 3600) were recently tested over a wide range of liquid/vapor (L/V) surface tensions using pure reference fluids acetone, isopropyl alcohol, methanol, and water, as well as binary mixtures of methanol and water. Pure reference fluid data are presented in Hartwig and Mann.[1] To obtain bubble point pressure data across the intermediate surface tension range between the alcohol-based pure liquids and water, binary mixtures of methanol and water were prepared at various methanol mass fractions. Interpretation of the solid/vapor (SV) and solid/liquid (SL) surface energies γ_{SV}, γ_{SL} is suggested through estimates using the Neumann equation of state.

Remark: Throughout this article, units of milli-Newtons per meter (mN/m) are used, rather than energy units for the various surface tensions; similarly the pressure is reported in units of Netwons per square meter (Pa).

Correspondence concerning this article should be addressed to J. Hartwig at Jason.W.Hartwig@nasa.gov.

Bubble Point Model

Hartwig and Mann[1] outlined a simplified bubble point model from the general Young–LaPlace equation for the pressure drop across a three-dimensional (3-D) curved interface

$$\Delta P_{BP} = \frac{4\gamma_{LV}\cos\theta_C}{D_p} \tag{1}$$

where ΔP_{BP} is the measured bubble point pressure, which is then taken as the differential pressure across the screen the moment when vapor penetrates a liquid laden porous screen, γ_{LV} is the liquid/vapor (L/V) surface tension, θ_C is the advancing contact angle between screen pore and liquid, and D_p is the effective pore diameter, which is fit to

$$\frac{1}{D_p} = \frac{1}{R_{max}} + \frac{1}{R_{min}} \tag{2}$$

where R_{max} and R_{min} are the principle radii of curvature at the L/V surface.

The effective pore diameter can be estimated through reference fluid bubble point tests (method 1), through historical bubble point data (method 2), or through scanning electron microscopy (SEM) analysis (method 3). Method 2 may be best despite added uncertainty in summing over all reported values, as summing over historical data takes into account sample to sample variations during screen manufacturing (Hartwig and Mann).[1] To make pretest predictions for a given LAD sample, obviously the best predictive tool is to conduct a reference fluid bubble point test for that exact sample, as in method 1. Method 3 has proven to be

Table 1. Comparison of Three Methods of Determining the Effective Pore Diameter: 1. Fit to Eq. 1 Using Pure Fluid Contact Angles, 2. Historical Data, and 3. SEM Analysis

	Pore diameter (μm)		
	Method 1	Method 2	Method 3
	Hartwig and Mann[1]	Historical	Based on SEM
325 × 2300	14.55 ± 0.3225	14.6 ± 0.55	14.8 ± 0.05
450 × 2750	11.65 ± 0.3225	11.8 ± 0.55	11.9 ± 0.05
510 × 3600	15.77 ± 0.3225	–	9.95 ± 0.05

unreliable because the complex 3-D pore diameter cannot be accounted through a simple 2-D projection at the screen face. As is evident in Table 1, the bubble point pressure does not scale with the mesh of the screen for pure fluids, as the 450 × 2750 screen outperformed the 325 × 2300, which outperformed the finest 510 × 3600 mesh using room-temperature liquids.

Stainless steels are complex mixtures of various components. During screen SEM analysis, qualitative composition measurements of each of the three meshes were made using energy dispersive x-ray microanalysis (EDAX) on both warp and shute wires. For all three screens, analysis showed that both wires were comprised of similar steel components, and that the ratios of metal components of the porous LAD screen, such as carbon, oxygen, nickel, and iron, were in direct proportion to a bulk 304SS sample, although not shown here.

Test Description

High-grade methanol (>99.5% pure) was purchased from a local chemical vendor, and standard distilled water was used to prepare binary reference fluid mixtures. Precise details of the experimental design and test procedure are outlined in the preceding article (Hartwig and Mann).[1] For binary mixture reference fluid testing, the following modifications were used.

Using graduated cylinders, water or methanol was added in known quantities to create a mixture at a known mass fraction of methanol, to submerge the LAD screen. Stirring rods were used to ensure uniform mixture composition. To change the mass fraction, a known amount of either methanol or water was simply added and mixed within the holding cylinder. Mixture tests would cease when the holding cylinder was nearly full. Cold ambient temperatures less than 277 K (40°F) in the test cell during bubble point tests ensured minimal evaporation of methanol from the mixtures. Then bubble point tests would commence; gaseous helium (GHe) was introduced beneath the LAD screen until breakthrough. The time at breakthrough was noted to compare with the time stamp in the data acquisition recording of the differential pressure across the screen. Then the GHe supply was decreased until screen reseal, and the process repeated again. At each methanol mass fraction, for each screen mesh, multiple points were recorded to ensure repeatability and consistency. At the end of each test, the screen and flange assembly was purged with dry GHe, the LAD screen was subject to a chemical bath, and the vertical holding cylinder was wiped clean and allowed to dry overnight.

Equation 1 relates experimentally obtained bubble points on the left side with theoretical predictions on the right side. To report bubble point values as a function of methanol mixture mass fraction, the following equation was used

$$\Delta P_{BP} = \Delta P_{DPT} - \rho_{mix}\, g h \tag{3}$$

where ΔP_{DPT} was the differential pressure measured across the screen, ρ_{mix} was the binary fluid mixture density, and h was the height of liquid on top of the LAD screen. The mixture density was calculated through precise knowledge of the added volume of methanol and water

$$\rho_{mix} = Y_{methanol}\, \rho_{meth} + (1 - Y_{methanol})\, \rho_{water} \tag{4}$$

where methanol and water densities were calculated from Hartwig and Mann[1] and methanol mass fraction was calculated from

$$Y_{methanol} = \frac{\rho_{meth} V_{meth}}{\rho_{meth} V_{meth} + \rho_{water} V_{water}} \tag{5}$$

To achieve a bubble breakthrough in the inverted configuration (liquid on top of the screen, gas on the bottom), the pressure underneath the screen was increased in fixed, quasi-static increments for precise pressure measurements and to allow a quasi-static equilibrium for the contact angle between the pore throat and solution and for the contact angle that is eventually pinned at the pore mouth. Bubble point was thus taken as the point when a visible gas bubble detached and broke away from the screen.

Theoretical Predictions

Pretest predictions were performed based on Eq. 1. To do so, knowledge of mixture surface tension, mixture contact angle, and effective pore diameters is required. Here, pore diameters were based on method 1 in Table 1, pure reference fluid bubble point tests. Mixture surface tension for all mass fractions was estimated from an equation of state and Langmuir isotherm[2] fit to data available in the literature. Mixture contact angles were measured as a function of methanol mass fraction.

Surface tension of methanol/water mixture at the air/solution and screen/solution interface

Surface tension values were previously measured at different mass fractions of methanol in water at constant temperature from 293 to 323 K, and are available in the literature.[3] Bubble point tests here were conducted over a colder range of temperatures (~275–295 K), so measurements from Ref. 2 at 293 K are used to predict all surface tension values for colder liquid. Surface tension data as a function of mass fraction of surfactant (methanol) at 293 K is plotted in Figure 1. Also plotted for comparison is the methanol/water surface tension data from Addesso and Lund.[4]

A Langmuir isotherm,[2] Eq. A25, is used to obtain a curve fit to the data for the purposes of predicting bubble point pressures at any mass fraction. The Gibbs equation using the convention that the excess volume and the excess of the solvent (water in this case) are set to zero, to satisfy the Gibbs phase rule that specifies the number of independent variables allowed in the representation of the surface tension of the binary solution of water and methanol. A brief derivation is presented in Appendix A; details are also available in Hansen[5] and Turkevich and Mann.[6] Figure 1 plots the Langmuir isotherm to the data of Vazquez[3] using these fitting parameters. Only the data from Vazquez[3] are included in the fit

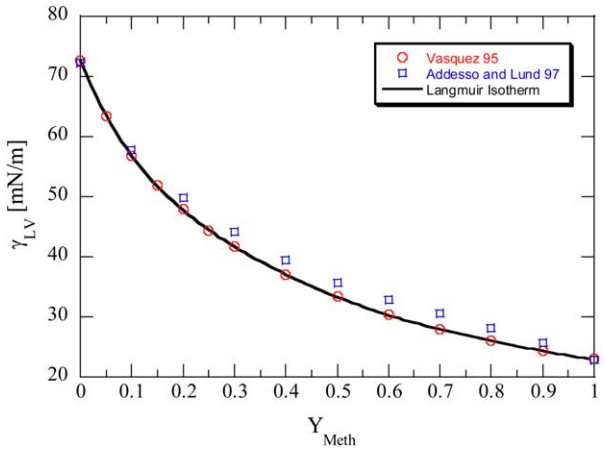

Figure 1. Experimental data and Langmuir isotherm fit to the $T = 20°C$ methanol/water surface tension data from Vazquez.[3]

The Langmuir isotherm parameters are (Eq. A24, Table 2) $\Gamma_{2,max} = 4.4$ molecules/nm^2, $a = 16.4$. [Color figure can be viewed in the online issue, which is available at wileyonlinelibrary.com.]

because data from Addesso and Lund[4] do not report a binary liquid temperature for their experiments.

Contact angle measurements

To the author's knowledge, no attempts have been made to measure contact angles on LAD screens, despite prior contact angle measurements of other binary liquids on other surfaces (eg., Li et al.[7]). A modified version of the Sessile Drop method was used to measure the advancing contact angle for mixtures with various methanol mass fractions. Details of the measurement are in Hartwig and Mann.[1] All solutions were prepared and mixed within a 100 mL glass graduated cylinder to measure liquid volume to within 1%.

Figure 2 plots the contact angle of methanol/water mixtures as a function of methanol mass fraction. Each data point represents the average of measurements at three independent, random locations on the screen surface. Also plotted is the methanol/water contact angle data from Addesso

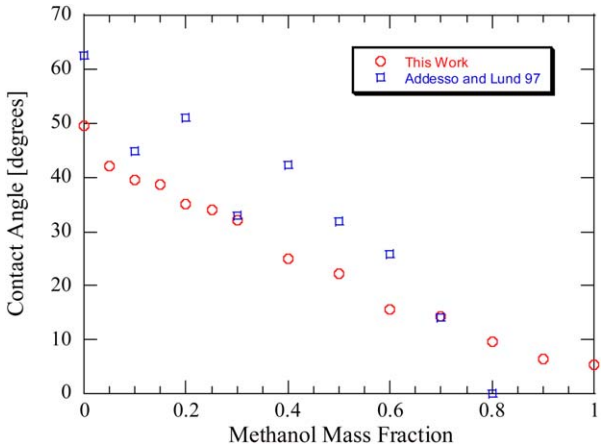

Figure 2. Contact angle measurements of water/methanol mixtures drops on the 325 × 2300 screen.

[Color figure can be viewed in the online issue, which is available at wileyonlinelibrary.com.]

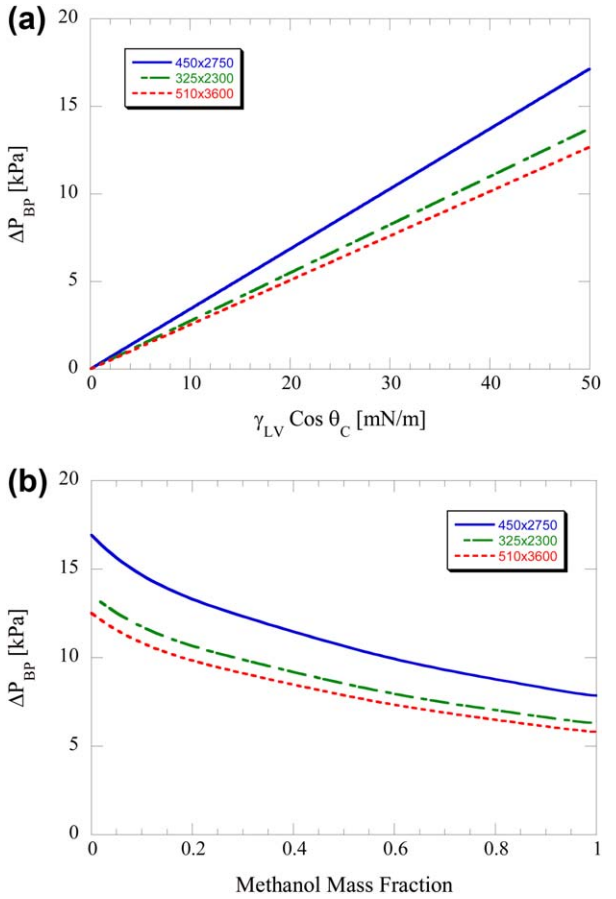

Figure 3. Bubble point predictions as a function of (a) mixture surface tension and (b) methanol mass fraction.

[Color figure can be viewed in the online issue, which is available at wileyonlinelibrary.com.]

and Lund[4] obtained using the Wilhelmy plate method. Reasonable agreement exists between the data sets. Methanol mass fraction values in this work were chosen consistent with mass fractions from bubble point measurements. Contact angle measurements for mixtures here are also in qualitative agreement with previously reported results from Fan et al.[8] for ethanol and *n*-propanol aqueous solutions.

Pretest predictions

Pretest predictions for the methanol/water binary mixture are plotted in Figure 3. As shown in Figure 3a, bubble point pressure scales with the contact angle corrected L/V surface tension of the liquid. The curvature tracks the surface tension data and contact angle measurements from Figure 2. Meanwhile, the predicted bubble point pressure scales with methanol mass fraction according to the curves in Figure 3b. Note that the 450 × 2750 mesh is predicted to outperform both 325 × 2300 and 510 × 3600 screen when using method 1 to specify the effective pore diameter (Hartwig and Mann).[1]

Results and Discussion

Bubble point pressure results

Figures 4a–6b plot experimental results for the binary mixture bubble point tests. Figures 4a, 5a, and 6a plot bubble point pressure as a function of the contact angle

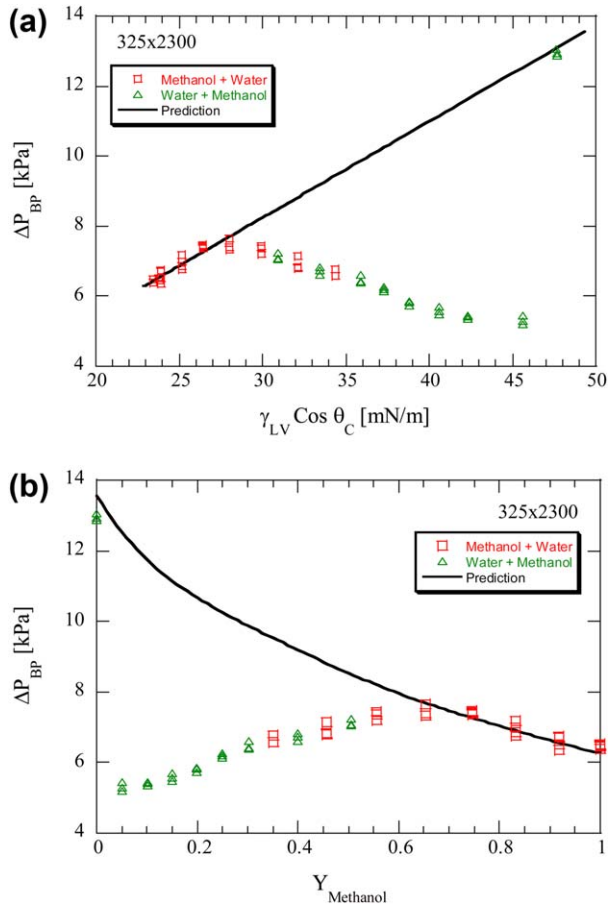

Figure 4. Bubble point pressure as a function of methanol/water mixtures as a function of (a) surface tension and (b) methanol mass fraction for the 325 × 2300 screen.

[Color figure can be viewed in the online issue, which is available at wileyonlinelibrary.com.]

corrected surface tension, and Figures 4b, 5b, and 6b plot the bubble point pressure as a function of the methanol mass fraction for the 325 × 2300, 450 × 2750, and 510 × 3600 screens, respectively. For each screen, tests were conducted beginning with pure methanol, then diluting with water, as well as tests beginning with pure water then diluting with methanol. The small overlap in methanol mass fractions allowed direct comparison between the two dilution techniques and ensured the data were independent of the chosen starting point. As shown, excellent agreement is obtained in the intermediate methanol mass fraction range as the data compare well between the two marching schemes. Theoretical predictions are based on pore diameters based on method 1 from Table 1.

As shown, the 450 × 2750 produces the highest bubble point pressure across the range of conditions. The coarser 325 × 2300 mesh outperforms the finest 510 × 3600 mesh, reiterating the fact that the bubble point pressure does not scale inversely with the fineness of the screen from Hartwig and Mann.[1] This may imply that the effective pore diameter is not only affected by the fluid, metal, and contact angle but also the specific geometry of the L/V interface within the screen pores. Nonetheless, a simple 2-D projection of a complex 3-D interface does not model the data and, thus, method 3 based on SEM analysis is again rejected.

To confirm that the performance gain using the 450 screen over the 510 screen was indeed true, and not due to faulty equipment or experimental apparatus, bubble point tests were again repeated a second time to ensure repeatability. No significant deviations in the results were noted. In addition, test hardware was inspected again. The screen samples were again analyzed under the SEM microscope to ensure consistency in warp and shute wire diameters all along the surface of the sample. No noticeable defects or deviations from the original measurements were noticed.

For all three screens, the data clearly deviate from the theoretical predicted value from Eq. 1 at methanol mass fractions less than 65%, even when the surface tension data are corrected for contact angle. Below methanol mass fractions of 65%, the only data point that matches with theoretical predictions is the pure water case. Figure 7 plots methanol mass fraction vs. methanol mole fraction. Comparing mass to mole fraction indicates that this apparent peak in bubble point at a mass fraction of 65% corresponds to a mole fraction of ~50% for the methanol/water mixtures from this work.

The disagreement between data and theory may be attributed to the following rationale: The screen is a porous object with millions of micron-sized holes, each with its own L/V interface. Statistically speaking, it is unlikely that every pore will have the same mixture composition at equilibrium. During pressurization underneath the screen, a bubble will pass

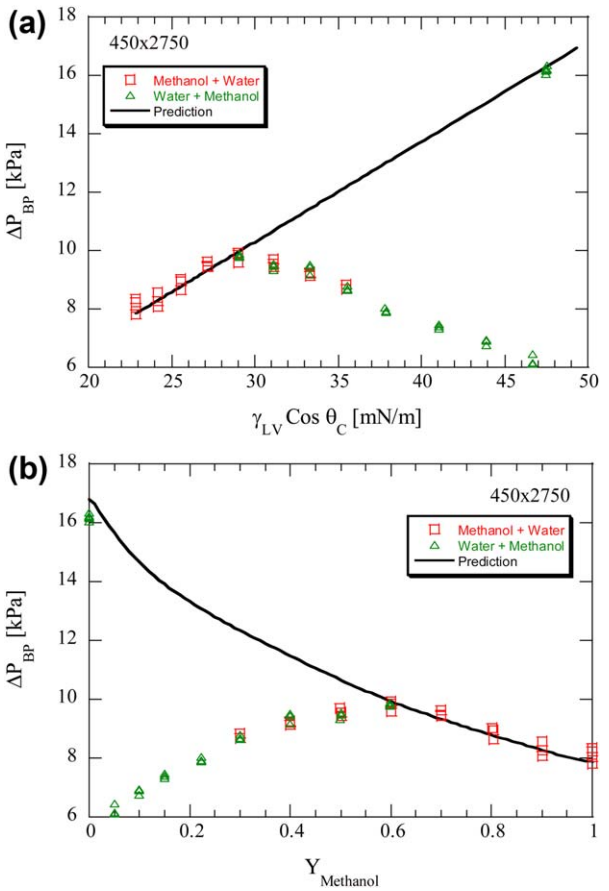

Figure 5. Bubble point pressure as a function of methanol/water mixtures as a function of (a) surface tension and (b) methanol mass fraction for the 450 × 2750 screen.

[Color figure can be viewed in the online issue, which is available at wileyonlinelibrary.com.]

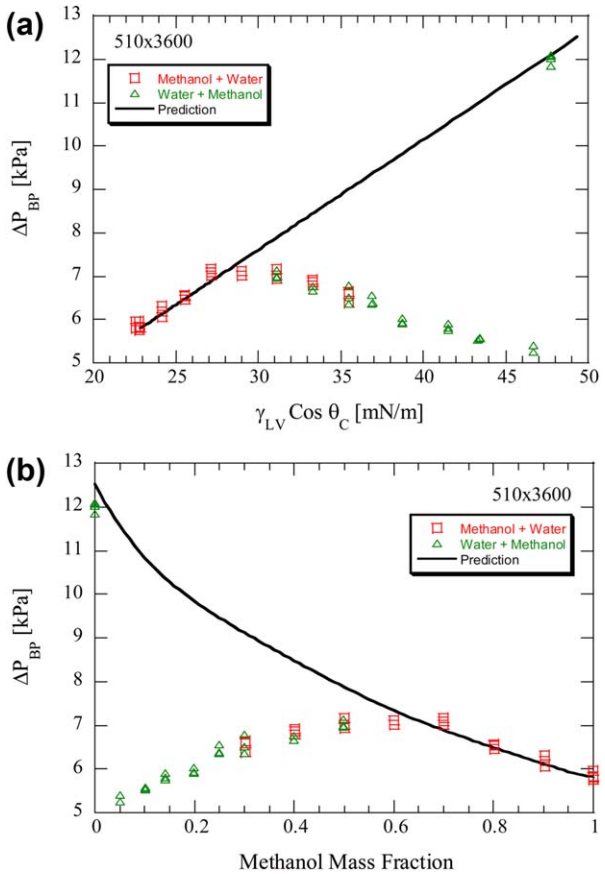

Figure 6. Bubble point pressure as a function of methanol/water mixtures as a function of (a) surface tension and (b) methanol mass fraction for the 510 × 3600 screen.

[Color figure can be viewed in the online issue, which is available at wileyonlinelibrary.com.]

through the largest pore that is occupied by the liquid with the lowest surface tension relative to other pores (i.e., simple path of least resistance). Results here indicate that the highest bubble point occurred when there was an equal distribution of methanol and water molecules at the liquid side of the interface. As the mixture dilutes toward pure water, the high contact angle of water and low surface tension of methanol dominate to produce lower than expected breakthrough pressures. Therefore, the data seem to indicate that methanol has a higher probability of populating an interface for this particular mixture. The article by Dougan et al.[9] provided a study that demonstrated the complex character of the structures that are found in methanol-water solutions at various mole fractions. They provided molecular dynamic simulations that suggest the possibility of doing simulations of the equilibrium states on a well-defined surface for a range of methanol concentrations. The implication of inhomogeneous solution of these room-temperature liquids at the screen thankfully has no effect on LAD performance in cryogenic liquids, because propellants are always stored in a homogenous, pure liquid state in the propellant tank.

Surface tension of methanol/water mixture at the SS/vapor and SS/solution interface

L/V surface tension values can be used to estimate S/V and S/L surface tensions of binary liquids from the classical force balance projected on the air/binary liquid mixture/SS304 screen pore interface as follows

$$F_{SL} - F_{SV} = -F_{LV}\cos\theta \tag{6}$$

This force balance assumes that the vertical component of the force is ignored, which resulted in a long and tangled history of dispute (Adamson and Gast[10]). For the Young–LaPlace equation, these forces are in direct proportion to the respective surface tensions

$$\gamma_{SL} - \gamma_{SV} = -\gamma_{LV}\cos\theta_C \tag{7}$$

where γ_{SL} and γ_{SV} are the SS304/solution and SS304/vapor surface tensions, respectively. The Young–LaPlace equation is considered valid for surfaces that are sufficiently hard so that there is a small normal displacement at the three-phase contact line. Although it is not possible to directly measure γ_{SL} or γ_{SV}, several algorithms based on the work of adhesion and the work of cohesion have been formulated to allow computation of γ_{SV} and γ_{SL} as a function of composition.

Consider the free energy change per unit area, known as the work of cohesion, defined as

$$\Delta G_C = 2\gamma_{SV} \tag{8}$$

The work of adhesion is defined as

$$W_a = \Delta G_a = \gamma_{LV} + \gamma_{SV} - \gamma_{SL} \tag{9}$$

Substituting Eq. 7 into Eq. 9

$$W_a = \gamma_{LV}(1+\cos\theta_C) \tag{10}$$

which permits direct computation of the work of adhesion using the known, measured binary mixture surface tension γ_{LV} and contact angle θ_C. The empirical equation of state analysis of Neumann and Spelt[11] is used to estimate γ_{SV}

$$\overline{W}_a = 2\sqrt{x}\exp\left(-\beta\gamma_{LV}^2(1-x)^2\right) \tag{11}$$

where $\overline{W}_a = \frac{W_a}{\gamma_{LV}}$ and $x = \frac{\gamma_{SV}}{\gamma_{LV}}$. Certain authors, for example, Li et al.[7] and Good,[12] comment that γ_{SV} should be independent of γ_{LV}, but this is often not observed. As the contact angle necessarily involves the three-phase contact line, the assumption of uniform chemical potentials requires that the composition of the vapor phase and, therefore, the magnitude of γ_{SV} must depend on Y_2.

Figure 8 plots the normalized work of adhesion, $\overline{W}_a$, of the SS304 system as a function of the L/V surface tension,

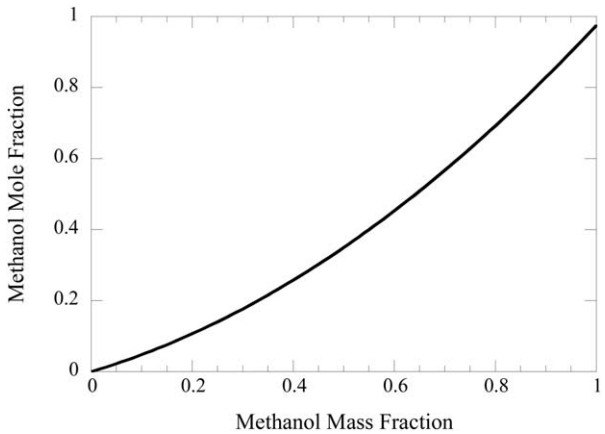

Figure 7. Methanol mole vs. mass fraction.

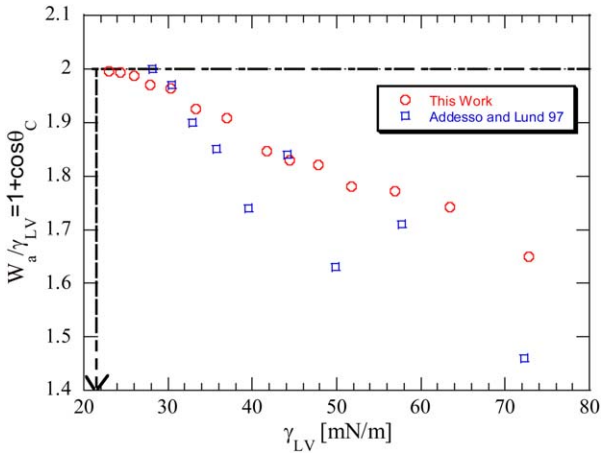

Figure 8. Zisman plot for binary methanol/water and SS304 system.

Here $\gamma_{CZ}=23.2\pm2\frac{mN}{m}$. [Color figure can be viewed in the online issue, which is available at wileyonlinelibrary.com.]

γ_{LV}. Also plotted for comparison is the methanol/water data from Addesso and Lund.[4] As shown in both data sets, the normalized work of adhesion varies with L/V surface tension; results from the current work show smoother variation to the contact angle data than that from Addesso and Lund.[4]

To obtain γ_{SV} as a function of γ_{LV}, Eq. 11 was solved numerically, given $\overline{W_a}$ and γ_{LV}. β is taken as 0.0001247 from Li et al.[7] Figure 9 shows results from this study, along with data from Ref. 3. It is clear from both data sets that γ_{SV} depends on γ_{LV} and that reasonable agreement exists between both sets despite two different 304SS compositions (i.e., solid steel plane vs. porous LAD screen).

Critical surface tension

Figure 8 is otherwise known as a Zisman plot.[13] By extrapolating to $1+\cos\theta_C \rightarrow 2$, one can obtain the so-called "critical" Zisman surface tension for a given solid material, where the contact angle approaches zero. This condition

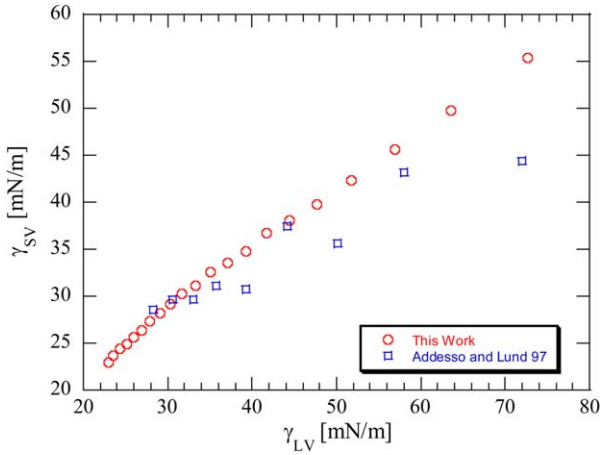

Figure 9. SV interfacial tension as a function of liquid/vapor interfacial tension for binary methanol/water and ss304 system.

[Color figure can be viewed in the online issue, which is available at wileyonlinelibrary.com.]

Table 2. Langmuir Isotherm Fitting Parameters

System	γ^0 (mN/m)	A_{MIN} (nm^2/molecule)	a
Solid–Vapor	55.4 ± 3.1	0.315 ± 0.030	11.3 ± 4.4
Solid–Liquid	6.12 ± 3.0	1.73 ± 0.20	33.5 ± 5.0
Liquid–Vapor	73.2 ± 3.4	0.22 ± 0.012	15.0 ± 8.0

defines the total wettability at the surface of the solid. Therefore, for $\gamma_{LV}<\gamma_{CZ}$, the contact angle is not expected to deviate from $\theta_C=0$ and the surface can be assumed to be completely wetted. Examination of data from this work indicates $\gamma_{CZ}=23.2\pm2\frac{mN}{m}$ for the porous LAD screen. This compares to $\gamma_{CZ}=24.8\pm5\frac{mN}{m}$ for a solid SS304 surface.[4] This may imply LADs screens demonstrate slightly improved wettability over nonporous SS due to the presence of the LAD screen pore.

The critical Zisman surface tension is anticipated to be only slightly dependent on temperature between room and liquid hydrogen temperatures. The temperature-dependent coefficient for the surface tension of the liquid and solid materials is negative so that the surface tension increases as the temperature is cooled below the critical temperature.[10] This property is difficult to measure in solids but is most probable that the solid-vapor surface tension of SS is at most somewhat larger at LH_2 temperatures than at room

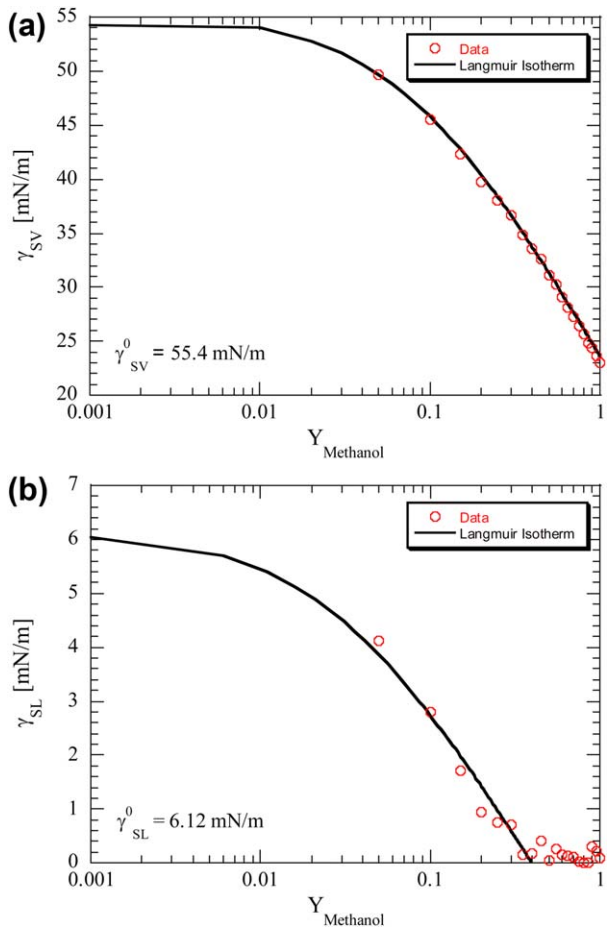

Figure 10. (a) SV and (b) SL interfacial tension as a function of methanol mass fraction.

[Color figure can be viewed in the online issue, which is available at wileyonlinelibrary.com.]

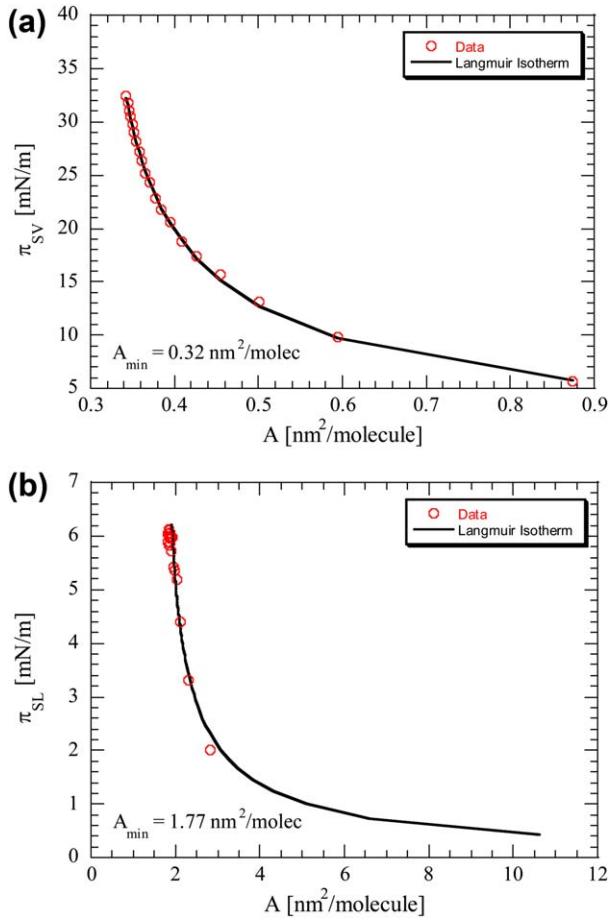

Figure 11. (a) SV and (b) SL spreading pressure as a function of "A."

[Color figure can be viewed in the online issue, which is available at wileyonlinelibrary.com.]

temperatures. This view is supported by the experimental results that the ΔP_{BP} vs. γ_{LV} is linear even though the temperature ranges between liquid hydrogen (20 K) and room temperature (~300 K). See Hartwig et al.[14]

Critical Zisman surface tension values obtained here have direct implications for predicting LAD behavior for cryogenic propellants. All cryogenic fluids of interest, including liquid helium, hydrogen, nitrogen, oxygen, and methane, have surface tension values less than the critical Zisman surface tension reported here. Results imply total wettability and that $\theta_C = 0$ for all cryogenic liquids with SS304 LAD screens, which further simplifies the bubble point model presented earlier.

The γ_{SV} and γ_{SL} isotherms

The formulas of Appendix B were used to first generate γ_{SV} from the Neumann equation of state as a function of Y_2. Then γ_{SL} vs. Y_2 was estimated by solving the Young–LaPlace equation. All Langmuir isotherm fitting parameters are reported in Table 2.

Figure 10 provides a contrasting picture of the variation of γ_{SV} and γ_{SL} with Y_2. The Langmuir isotherm fits the γ_{SV} data very well throughout the range of concentrations studied. Moreover $\gamma_{SV} \in [23, 55.4)\text{mN/m}$ is substantially larger than the range $\gamma_{SL} \in [0, 6.12)\text{mN/m}$. The fit to the SV data is excellent, but the fit to the SL data is modest up to $Y_2 = 0.4$; the data between (0.4, 1] did not follow the fit. The nonlinear least-squares procedure could not be made to converge when the γ_{SL} data for $Y_2 > 0.4$ was included in the array. Apparently, the structure of the solution–SS304 interface does not satisfy the conditions required for the Langmuir isotherm to be valid.

Figure 11 uses the result of computing $A^{SX} = 1/\Gamma_2^{SX}$ from Eq. B3. The co-area, $A_{\min}$, for the solid-vapor interface is reasonable when compared to close packing of long-chain alcohols, which are in the range of $(0.2, 0.3)\text{nm}^2/\text{molecule}$. The co-area found for the solid-liquid is sufficiently large that the solid-liquid interface may be mostly water clusters with only a relatively few methanol molecules at the surface; the co-area ratio is 5.5.

A question is whether the completely soluble methanol-water solution has local structures analogous to microemulsions. Dougan et al.[9] built a case for the possibility that methanol-water mixtures are not homogenous but tend to form clusters of various sizes. Their data suggest that at higher concentrations of methanol "the system segregates into what is effectively a molecular-scale microemulsion." They provide evidence that in the concentration range $Y_2 \in (\sim 0.27, 0.54)$ "both water and alcohol clusters percolate simultaneously." This is analogous to the bicontinuous structures that manifest in microemulsions in certain regions of their phase diagrams.

Conclusions

Bubble point tests conducted in methanol/water mixtures are in agreement with pure reference fluid tests in that the 450 × 2750 again outperformed the 325 × 2300 and 510 × 3600 meshes. Experimental data and prediction values based on pore diameters based on the pure reference fluids match well for methanol mole fractions greater than 50%; for methanol mole fractions less than 50%, the data deviate from theory. Care was taken during testing to ensure adequate bulk mixing of the fluids, but this discrepancy is likely attributable to small differences in mixture composition within the micron-sized pores, as this is backed by Dougan et al.[8] As the mixture tends toward higher water concentrations, the low surface tension of methanol and high contact angle of water dominate and occupy the breakthrough sites.

A critical Zisman L/V surface tension value of $\gamma_{CZ} = 23.2 \pm 2\,\frac{\text{mN}}{\text{m}}$ is defined for these screen channel LADs. All cryogenic L/V surface tensions lie well below this critical value. Therefore, the implication is that one can confidently assume zero contact angle between SS304 LAD screens and all cryogenic liquids.

The bubble point tests conducted in methanol/water mixtures were worked up to show properties of the three-phase interfaces along the complex contact line in SS304 LAD screens. In particular, the variation with Y_2 of the solid-vapor γ_{SV} differed from that of the solid-liquid interface γ_{SL}. The data are consistent with the Langmuir isotherm description of the thermodynamics of adsorption. The result of the analysis is that the co-areas, $A_{\min}$ are 0.32 nm^2/molecule for the SS304–vapor interface and 1.77 nm^2/molecule for the SS304–solution interface. This implies that that methanol molecules form a dense, liquid-like monolayer at the interface of SS304 with the vapor phase, while the methanol molecules are very dilute in the interface between SS304 and the solution of methanol-water.

Literature Cited

1. Hartwig JW, Mann JA. A Predictive bubble point pressure model for porous liquid acquisition devices. *J Porous Media*. 2014 (in press).
2. Langmuir I. The constitution and fundamental properties of solids and liquids. Part I. Solids. *J Am Chem Soc*. 1916;38:2221–2295.
3. Vazquez G, Alvarez E, Navaza JM. Surface tension of alcohol + water from 20 to 50°C. *J Chem Eng Data*. 1995;40:611–614.
4. Addesso A, Lund DB. Influence of solid surface energy on protein adsorption. *J Food Process Preserv*. 1997;21:319–333.
5. Hansen RS. Thermodynamics of interfaces between condensed phases. *J Phys Chem*. 1961;66:410–415.
6. Turkevich LA, Mann JA. Pressure dependence of the interfacial tension between fluid phases. Formalism and application to simple fluids. *Langmuir*. 1990;6:445–456.
7. Li D, Ng C, Neumann AW. Contact angles of binary liquids and their interpretation. *J Adhes Sci Technol*. 1992;6:601–610.
8. Fan L, Yuan X, Zhou C, Zeng A, Yu K, Kalbassi M, Porter K. Contact angle of ethanol and n-propanol aqueous solutions on metal surfaces. *Chem Eng Technol*. 2011;34:1535–1542.
9. Dougan L, Bates SP, Hargreaves R, Fox JP, Crain J, Finney JL, Reat V, Soper AK. Methanol-water solutions: a bi-percolating liquid mixture. *J Chem Phys*. 2004;121(13):6456–6462.
10. Adamson AW, Gast AP. Physical Chemistry of Surfaces. New York: Wiley, 1997.
11. Neumann AW, Spelt JK. Applied Surface Thermodynamics. New York: Marcel Dekker, 1996.
12. Good RJ. Surface free energy of solids and liquids: thermodynamics, molecular forces, and structure. *J Colloid Interface Sci*. 1976;59:398–419.
13. Zisman WA. Contact angle, wettability, and adhesion. *Adv Chem Ser*. 1974;43:1–51.
14. Hartwig JW, McQuillen JB, Chato DJ. Performance gains of propellant management devices for liquid hydrogen depots. In: AIAA-2013-0368, 51st Annual Meeting of the Aerospace Sciences. Grapevine, TX, January 7–10, 2013.
15. Neumann AW, Good RJ. Techniques of measuring contact angles. *Surf Colloid Sci*. 1979;11:31–91.

Appendix A: Langmuir Isotherm for the Liquid/Vapor Case

Starting with the combined form of the first and second law of thermodynamics for the diluted system, which takes into account the energy at the L/V interface

$$dU = TdS - PdV + \sum_{i=1}^{c} \mu_i dn_i + \gamma_{LV} dA \tag{A1}$$

for a system that consists of two phases, α and β. Integrating, the Euler equation is obtained

$$U = TS - PV + \sum_{i=1}^{c} \mu_i n_i + \gamma_{LV} A \tag{A2}$$

for the entire system phase α, the interface, and phase β. From Eqs. A1 and A2, the Gibbs–Duhem equation is obtained

$$0 = SdT - VdP + \sum_{i=1}^{c} n_i d\mu_i + Ad\gamma_{LV} \tag{A3}$$

where S, V, n_i are extensive variables that include all of phases α, β, and the interface of area A. Note that Eq. A3 without constraints does not obey the Gibbs phase rule, which counts the number of independent intensive variables $f = 2 + c - p = c$. Any two of the set of intensive variables $T, P, \{\mu_i\}_{i=1}^{c}$ must be dependent variables along with the L/V surface tension γ_{LV}. A number of algorithms exist for eliminating two of the dependent variables. The method of Hansen[4] and Turkevich and Mann[5] is used, and the method of undetermined multipliers is used asserting two conditions, one for each phase. The first condition is that of thermal, mechanical, and chemical equilibrium so that each of the variables $T, P, \{\mu_i\}_{i=1}^{c}$ are uniform throughout phases α, β, and the interface. Then two conditions are satisfied

$$\begin{aligned} 0 &= S^{\alpha v} dT - dP + \sum_{i=1}^{c} c^{a}{}_{i} d\mu_i, \\ 0 &= S^{\beta v} dT - dP + \sum_{i=1}^{c} c^{\beta}{}_{i} d\mu_i \end{aligned} \tag{A4 and A5}$$

Let the undetermined multipliers be λ^{α} *and* λ^{β} so that adding Eqs. A4 and A5 to A3 gives

$$\begin{aligned} 0 = &(S - \lambda^{\alpha} \overset{v}{S^{\alpha}} - \lambda^{\beta} \overset{v}{S^{\beta}}) dT - (V - \lambda^{\alpha} - \lambda^{\beta}) dP \\ &+ \sum_{i=1}^{c} (n_i - \lambda^{\alpha} c_i^{\alpha} - \lambda^{\beta} c_i^{\beta}) d\mu_i + A d\gamma \end{aligned} \tag{A6}$$

where the area of the interface and the volumes of the phases are arbitrary. Define the excess quantities $S^e, V^e, \{n_i^e\}_{i=1}^{c}$ by

$$\begin{aligned} S^e &= S - \lambda^{\alpha} S^{\alpha v} - \lambda^{\beta} S^{\beta v} \\ V^e &= V - \lambda^{\alpha} - \lambda^{\beta} \\ n_i^e &= n_i - \lambda^{\alpha} c_i^{\alpha} - \lambda^{\beta} c_i^{\beta} \end{aligned} \tag{A7-A9}$$

The two side conditions are taken into account and, therefore, the phase rule is satisfied by setting any two functions S^e, V^e, n_i^e equal to zero and solving for $\lambda^{\alpha}, \lambda^{\beta}$. The selection is made for convenience; different conventions will be used for the liquid-vapor interfacial system and for the solid-vapor or solid-solution interfacial systems. Dividing by the area A, results in a formula for the differential of γ_{LV}

$$-d\gamma = \overline{S} dT - \tau dp + \sum_{i=1}^{c} \Gamma_i d\mu_i \tag{A10}$$

Subject to setting to zero any two of the excess coefficients $(\overline{S}, \tau, \{\Gamma_i\}_1^c)$; τ is the Hansen excess volume per unit area of the interface.[5,6] This formula is valid regardless of whether the phases are solids, liquids or gases. It is common practice to use tension units of milli-Newtons per meter for γ_{LV} when the interface is between liquid phases or liquid-fluid phases and energy units milli-Joules per square meter when one phase is a solid. The units of γ_{LV} [=]mN/m are used for all interfacial tensions, including γ_{SV}, γ_{SL}.

Consider first the L/V interface (Figure 1) and in this case, the classical convention of Gibbs is used to set $V^e = 0, n_1^e = 0$ in which case, Eq. A11 is obtained after dividing through by the area of the interface, and rearranging

$$-d\gamma_{LV} = \overline{S} dT + \sum_{i=2}^{c} \Gamma_i d\mu_i \tag{A11}$$

where $\overline{S}$ is the excess entropy per area and $\{\Gamma_i\}_2^c$ are the excess of compositions per unit area at the interface, excluding the majority component (labeled as i=1). Therefore, one can define these excesses in terms of partial derivatives

$$\overline{S} = -\left(\frac{\partial \gamma_{LV}}{\partial T}\right)_{\{\mu_i\}_2^c}, \Gamma_i = -\left(\frac{\partial \gamma_{LV}}{\partial \mu_i}\right)_{T, \{\{\mu_i\}_2^c - \mu_1\}} \tag{A12 and A13}$$

In the Gibbs convention, for a two component system of solvent, $i = 1$ (water), and solute, $i = 2$ (methanol), Eq. A11 becomes

$$-d\gamma_{LV} = \overline{S} dT + \Gamma_2 d\mu_2 \tag{A14}$$

Evaluating subcooled liquid states for bubble point tests would involve an added complexity, as one would have to take into account the pressure dependence of the surface tension.[6] Therefore, to permit facile interpretation of the data, reference fluid bubble point tests are conducted in equilibrium saturated liquid states. One can then use Eqs. A12–A14 to determine the excess of composition of methanol

$$\Gamma_{\text{meth}} = -\left.\frac{\partial \gamma_{\text{LV}}}{\partial \mu_{\text{meth}}}\right|_{\text{T,P}} \tag{A15}$$

The chemical potential can be written as

$$\mu_{\text{meth}} = \mu^0_{\text{meth}} + kT \log (a_2) \tag{A16}$$

where k is the Boltzmann constant, a_2 is the activity of component 2, methanol in this case, which can be written as the product of the activity coefficient α_2 and the concentration, Y_2 is the mass fraction of methanol

$$\mu_{\text{meth}} = \mu^0_{\text{meth}} + kT \log (\alpha_2 Y_2) \tag{A17}$$

The assumption is made that $a_2 \approx 1$ even though $Y_1 \in [0, 1]$. The goodness of fit to the Langmuir isotherm supports this assumption. Substituting Eq. A17 into Eq. A15

$$\Gamma_2 = -\left.\frac{\partial \gamma_{\text{LV}}}{\partial (kT \log Y_2)}\right|_{T,P} \tag{A18}$$

Simplifying

$$\Gamma_2 = -\frac{1}{kT}\left.\frac{\partial \gamma_{\text{LV}}}{\partial (\log Y_2)}\right|_{T,P} \tag{A19}$$

To determine Γ_2 vs $.Y_2$, an equation of state is required; the Langmuir isotherm is used herein to fit the various data sets

$$\Gamma_2 = \Gamma_{2,\max} \frac{aY_2}{1+aY_2} \tag{A20}$$

where a and $\Gamma_{2,\max}$ are fitting parameters. Inserting Eq. A20 into Eq. A19 and rearranging

$$-d\gamma_{\text{LV}} = kT\Gamma_{2,\max}\, d\log (1+aY_2) \tag{A21}$$

The "spreading pressure" can now be defined

$$\pi = \gamma^0_{\text{LV}} - \gamma_{\text{LV}} \tag{A22}$$

where γ^0_{LV} for the liquid-vapor system is the surface tension of water without methanol present, $Y_2 = 0$. Computing the differential of both sides of Eq. A22

$$d\pi = -d\gamma_{\text{LV}} \tag{A23}$$

So that

$$d\pi = kT\Gamma_{2,\max}\, d\log (1+aY_2) \tag{A24}$$

Integrating Eq. A24 from $Y_2 = 0$ to Y_2

$$\pi = kT\Gamma_{2,\max} \log (1+aY_2) \tag{A25}$$

The fitting equation is then

$$\gamma_{\text{LV}} = \gamma^0_{\text{LV}} - kT\Gamma_{2,\max} \log (1+aY_2) \tag{A26}$$

Since $\gamma_{\text{LV}}, T, Y_2$ are known in discrete intervals, Eq. A26 can be used to determine the three fitting parameters γ^0_{LV}, a, and $\Gamma_{2,\max}$ by a nonlinear fitting algorithm, which was applied to the $T = 20°\text{C}$ methanol/water data from Vazquez.[2] Fitting the Langmuir isotherm through the data yields

$$\Gamma_{2,\max} = \frac{4.44 \text{ molecules}}{\text{nm}^2}$$

$$a = 16.4$$

After inserting these values into Eq. A26 and rearranging, a Langmuir isotherm is generated, which allows prediction of mixture fluid bubble points at any methanol mass fraction. Note that $A_{2,\min} = \frac{1}{\Gamma_{2,\max}} = 0.23 \frac{\text{nm}^2}{\text{molecule}}$, which suggests that the air/water interface is covered by a methanol monolayer that is packed. Compare this number to the co-area of a close-packed monolayer of a long-chain alcohol of $0.20 \frac{\text{nm}^2}{\text{molecule}}$ at the solution/water interface.[6] This result suggests the possibility of a considerable adsorption of methanol at the SS304/solution interface. Fan et al.[8] provides experimental data from neutron diffraction studies along with molecular dynamic simulation that show that, even though water and methanol mix in all proportions, there are extended structures that transform into "bipercolating liquid mixtures." The surface structure may be quite complex. The fact that the Langmuir isotherm does so well in fitting the experimental data is an interesting result.

Appendix B: Langmuir Isotherm for the SL and SV Cases

The Langmuir isotherm, γ_{LV} vs $.Y_2$ for the methanol-water solution against its vapor can be measured directly, and the Langmuir parameters determined as described in Appendix A. However, the dependent variables, γ_{SV} and γ_{SL}, are not directly determined by experiment but can be computed in the following manner using the equation of state analysis from Ref. 15.

Direct macroscopic measurement of the contact angle of methanol-water mixtures can be performed on the SS304 porous screens. It is then possible to compute the work of adhesion invoking the Young–Laplace equation. Once the work of adhesion is determined, an equation of state is invoked to estimate γ_{SV}. Given $(\gamma_{\text{LV}}, \gamma_{\text{SV}})$ vs. Y_2, γ_{SL} can be estimated as a function of Y_2 by invoking the Young–LaPlace equation (Eq. 7). As the structure of the SS304 surface is unknown with respect to the adsorption of methanol or water components, a molecular level interpretation of the isotherms will not be attempted. EDAX data were collected on the screens used in this study, which showed that the distribution of chemical elements (Carbon, Nickel, Iron, etc.) on the surfaces of the screens was consistent at any location on the screen, and that the composition breakdown as expected for a SS304 piece of material.

From an engineering viewpoint, it is asserted that a lumped parameter, C_{SS304}, is sufficient to represent this complex system in Eq. A11 such that

$$-d\gamma = \overline{S}dT - \tau dp + \Gamma_{\text{meth}}\, d\mu_{\text{meth}} \tag{B1}$$

where $\Gamma_{\text{SS304}} = 0$ and $\Gamma_{\text{water}} = 0$, which satisfies the phase rule, even though the analytical chemistry of component distribution in the SS304 phase and of SS304 components in the other phases is unknown. The pressure term is negligible, since $\tau = \left.\frac{\partial \gamma}{\partial p}\right|_{T,\mu_{\text{meth}}}$ is small for the liquid and solid phases.[5] The experiments were done at constant temperature so that the working differential form is

$$-d\gamma = \Gamma_{\text{meth}}\, d\mu_{\text{meth}} \tag{B2}$$

And, therefore, the fitting equation is

$$\gamma_{\text{SX}} = \gamma^0_{\text{SX}} - kT\Gamma^{\text{SX}}_{2,\max} \log \left(1+a^{\text{SX}} Y_2\right) \tag{B3}$$

where SX represents either the solid-liquid interface, SL, or the solid-vapor interface, SV. Once the parameters $\gamma^0_{\text{SX}}, \Gamma^{\text{SX}}_{2,\max}, a^{\text{SX}}$

are determined by fitting Eq. B3, the two excesses can thus be estimated by the Langmuir isotherm, Eq. A20, written as

$$\Gamma_2^{SX} = \Gamma_{2,max}^{SX} \frac{a^{SX} Y_2}{1 + a^{SX} Y_2} \tag{B4}$$

The parameters obtained from the fitting equation will differ depending on the interface, liquid-vapor, SS304–vapor, or SS304–solution, see Table 2.

The correlation of the contact angle data for binary fluids with the "surface energy" of solids is not clear experimentally. For example, Good,[12] in his Kendall award lecture cautioned against the use of liquid mixtures to span the L/V surface tension range required to estimate solid surface free energies. More recently, Li et al.,[7] reported inconsistent results of advancing, Sessile drop contact angles and the estimation of γ_{SV} using binary liquid mixtures.

Assume that $\mu_2^{solution} = \mu_2^{Vapor}$ and that the activity coefficients, $\alpha_i = 1$. Remark: While the activity coefficient of methanol deviates from unity at small mole fractions, the data analyzed is in a concentration range in which $\alpha_2 \approx 1$ is a close enough approximation to see the effects of adsorption. As $\overline{W}_a$ vs. γ_{LV} was established experimentally, Eq. 11 was solved for γ_{SV} vs. Y_2 by a direct search algorithm. Tables of π_{SV} vs. A_{SV} and π_{SL} vs. A_{SL} were constructed, where $A_{SX} = 1/\Gamma_2^{SX}$. Note that Γ_2^{SV} or Γ_2^{SL} are determined from the Langmuir isotherm using the coefficients given in Table 2.

Note: The uncertainties quoted here are derived from the least-squares algorithm. The residuals are small enough to suggest good fits but in each case the condition numbers were rather large and the uncertainties reflect that property. The fit of the solid-liquid isotherm required special care to obtain convergence; the methanol-water cluster structure of the composition range above 0.4 mass fraction is of interest.

Manuscript received Oct. 22, 2013, and revision received May 29, 2013.